

# Lane Formation in a Microscopic Model and the corresponding Partial Differential Equation

Jan-Frederik Pietschmann  
DAMTP, University of Cambridge,  
Cambridge CB3 0WA, UK [J.Pietschmann@damtp.cam.ac.uk](mailto:J.Pietschmann@damtp.cam.ac.uk)

Bärbel Schlake  
Institut für Numerische und Angewandte Mathematik  
Westfälische Wilhelms-Universität Münster  
[baerbelschlake@wwu.de](mailto:baerbelschlake@wwu.de)

## Abstract

*We study the lane formation capabilities of a cellular automaton model introduced by [A. Kirchner and A. Schadschneider: Simulation of evacuation processes using a bionics-inspired cellular automaton model for pedestrian dynamics. Physica A: Statistical Mechanics and its Applications, 312(1-2):260–276, 2002]. We present numerical examples demonstrating the formation of lanes in the microscopic setting. Using the link to a macroscopic partial differential equation, we are able to give conditions on the stability of perturbations corresponding to the formation of lanes in the microscopic case.*

## 1. Introduction

The formation of lanes in two groups moving in opposite directions is a famous and important example of self-organisation in human crowds. Pedestrians with the same desired walking direction prefer to walk in lanes. Typically, the number of lanes depends on the width of the street and on the density of pedestrians. The explanation for lane formation is as follows: Pedestrians walking against the stream have a high relative velocity. As a consequence, pedestrians change their walking direction sideways to avoid collisions, which finally leads to separation [8]. Such effects are commonly observed in pedestrian dynamics [10], [7]

We study the lane formation capabilities of a cellular automaton model for human crowd motion introduced in [12]. In this model, the crowd is considered as a group of a finite number of individuals living on a rectangular two-dimensional grid. Given a discrete time step, the model provides for each individual in a given cell the probability to jump into a neighbouring cell. This probability is

determined by several factors: First of all, individuals are not allowed to jump to an occupied cell (size exclusion, cf. [17]). Furthermore, there exist two driving forces, called "floor fields", cf. [4], a static field  $S$  and a dynamic field  $D$  on which the jump-probability depends exponentially. The static field  $S$  provides individuals with a sense of their environment, increasing towards locations they want to reach, such as doors. The dynamic field  $D$  is created by the particles themselves and accounts for herding effects. This is a key feature of the model and one goal of this paper is to examine its impact on the formation of lanes. Being zero at the initial time, the value of  $D$  is increased whenever a particle leaves a cell, modelling the tendency of people to follow others. It is straightforward to extend this model to multiple species, each of them coupled to its own dynamic and static field. We remark that lane formation is created by pedestrians via self-organisation. In our model, we do not assume that individuals have a tendency to prefer a special walking site. We consider the case of two species (labelled red or  $r$  and blue or  $b$  in the following) and focus on the formation of lanes. The formation of lanes for two species (but without static field) has already been briefly demonstrated in [15]. Here, we shall present the results of Monte Carlo simulations showing the formation of lanes. The main part will be to analyse the corresponding continuum partial differential equation model. For one species, this limit has already been considered, cf. [2]. We shall exploit linear stability properties of this model yielding insight into the role of the dynamic fields for the formation of lanes.

## 2. Related Work

In the modelling of human crowds, one can distinguish between two general approaches: microscopic and macroscopic models. In the microscopic framework people are

treated as individual entities (particles) while in the macroscopic description the crowd is represented by a density function and it is no longer possible to observe individual entities. The evolution of the particles in time is determined by physical and social laws which describe the interaction among the particles as well as their interactions with the physical surrounding. Examples of microscopic methods are social-force models (see [9] and the references therein), queuing models e.g. [21] or continuum dynamic approaches like [19]. For an extensive review of different microscopic approaches we refer to [6]. We are interested in the cellular automation model [15], see [5, 14] for other examples. It has been demonstrated in a number of papers, cf. [1, 18, 17], that it is possible to derive macroscopic partial differential equation from these models by a formal limit process. As in [2], we are interested in comparing these two formulations numerically.

### 3. The Microscopic Model for Two Species

The model under consideration is based on an Asymmetric Simple Exclusion Process (ASEP) on a two-dimensional grid of size  $m_x \cdot n_y$  (the size of one cell is typically about  $40 \times 40 \text{ cm}^2$ , cf. [16], originating from a maximal density of 6.25 people per  $m^2$ , cf. [20]). For simplicity, we shall only explain the model for particles of group  $r$  with corresponding fields  $D_r$  and  $S_r$ . The probability of a particle to jump into a neighbouring cell  $i, j$  is given by

$$(P_r)_{i,j} = (N_r)_{i,j} \exp(k_D (D_r)_{i,j}) \exp(k_S (S_r)_{i,j}) \times (1 - r_{i,j} - b_{i,j}). \quad (1)$$

The term  $(1 - r_{i,j} - b_{i,j})$  accounts for the size exclusion effect rendering the probability zero if a cell is occupied. The positive constants  $k_D$  and  $k_S$  regulate the relative influence of the two floor fields. Finally,  $(N_r)_{i,j}$  is a normalisation factor given by

$$(N_r)_{i,j}^{-1} = \sum_{k=\{i-1, i+1\}} \sum_{l=\{j-1, j+1\}} e^{k_D (D_r)_{k,l}} e^{k_S (S_r)_{k,l}}. \quad (2)$$

The dynamic fields  $D_r$  is zero at the beginning of a simulation. In every step, it is updated using the following rules

- It is increased by one whenever a particle left a cell, i.e.

$$(D_r)_{i,j}^{k+1} = \begin{cases} (D_r)_{i,j}^k + 1 & \text{if } (r_{i,j}^k - r_{i,j}^{k+1}) = 1 \\ (D_r)_{i,j}^k & \text{otherwise} \end{cases} \quad (3)$$

- If  $D_r \geq 1$ , it decreases by a given probability  $\delta > 0$ , i.e. given a random number  $p$

$$(D_r)_{i,j}^{k+1} = \begin{cases} (D_r)_{i,j}^k - 1 & \text{if } p < \delta \\ (D_r)_{i,j}^k & \text{otherwise} \end{cases} \quad (4)$$

- The diffusion is implemented in the following way: With a probability of  $\kappa/4$ ,  $\kappa \in \mathbb{R}_+$  a particle jumps to one of its neighbouring fields. With probability  $(1 - \kappa)$ , it stays at its place.

Note that these rules imply that the value of  $D_r$  is always a non-negative integer.

### 4. Monte Carlo Simulations

We performed simulations of the above model on a  $20 \times 100$  cell grid. We used a Mersenne twister, cf. [13], to create the pseudo-random numbers needed. The main issue here is to deal with so-called ‘‘conflicts’’, i.e. the case when two particles want to jump into the same cell. In our implementation, we followed the strategy described in [11]. The basic idea is the following: A new parameter  $\lambda \in [0, 1]$  is introduced. If two or more particles want to jump to the same cell, this new parameter determines their behaviour: With probability  $\lambda$ , none of the particles jumps and the cell remains empty. With probability  $(1 - \lambda)$ , one particle is chosen randomly and jumps into the target cell. In our set-up, red particles enter the domain from the left and blue particles from the right. Both species are supplemented with a static field transporting them through the channel. For this simulation, we chose the following parameters:  $\delta = 0.05$ ,  $k_D = 1.0$ ,  $k_S = 7$ ,  $\kappa = 0.5$ . The diffusion coefficients of  $r$  and  $b$  are chosen as 0.0005 in  $x$ - and 0.1 in  $y$ -direction. The boundary conditions are implemented as follows: In each step, for each cell on the left boundary, a random number is generated. If this number is below a given value  $b_{c_l}$ , a virtual particle is created. This particle evolves due to the usual probabilities given by the model and can either jump into the domain or vanishes. On the right side, the boundary conditions are implemented in the same way with a corresponding boundary value  $b_{c_r}$ . In our experiment, we added small perturbations in  $y$ -direction, i.e.

$$b_{c_l} = \tilde{b}_{c_l} + 0.04 \sin\left(\frac{2k\pi}{n_x} i\right), \quad i = 1, \dots, n_x, \quad (5)$$

$$b_{c_r} = \tilde{b}_{c_r} + 0.04 \sin\left(\frac{2k\pi}{n_x} i + \pi\right), \quad i = 1, \dots, n_x. \quad (6)$$

Here, we chose  $\tilde{b}_{c_l} = \tilde{b}_{c_r} = 0.06$ . In Figure 1 (top), we show a snapshot of one simulation demonstration the formation of two lanes. Figure 1 (bottom), we show the average density of red particles at step 2000 averages over 35 simulations, in Figure 1 (middle), we same is shown for the blue species.

### 5. The Macroscopic PDE Limit

Following the strategy described in [1, 17] it is straightforward to obtain a continuum PDE limit of the above cellular model. The densities of the two species are labelled  $r$

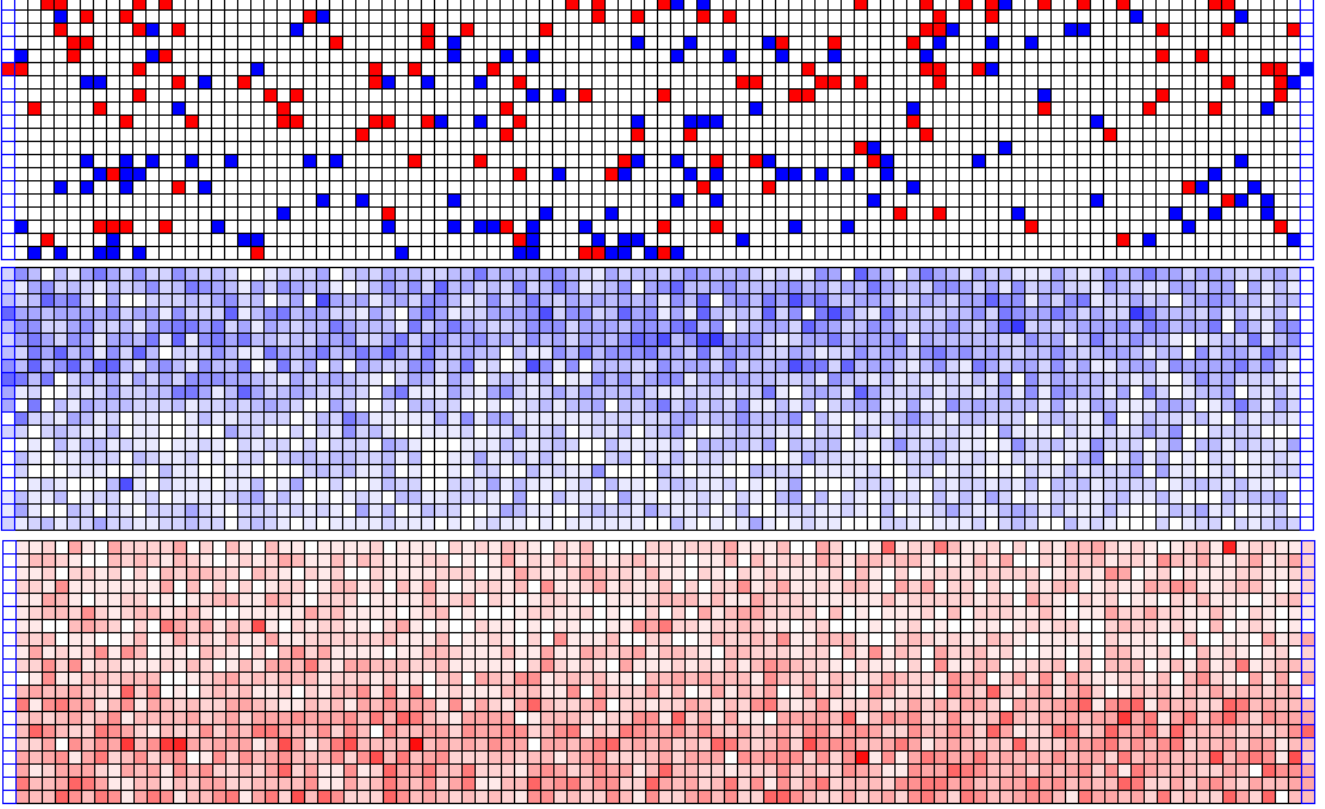


Figure 1. Results of the Monte Carlo Simulations: Snapshot of a single Simulation after 1000 steps (top); Density of red particles after 2000 steps, averages over 35 runs (bottom); Density of blue particles after 2000 steps, averages over 35 runs (middle).

and  $b$ ,  $P \in \mathbb{R}^+$  denotes their diffusion coefficient,  $\rho = r + b$  denotes the total mass,  $S_r$  and  $S_b$  denote external potentials and  $D_r$  and  $D_b$  denote the dynamic fields. As a result we obtain the following non-linear Nernst-Planck type equations

$$\partial_t r = \nabla \cdot P((1 - \rho)\nabla r + r\nabla \rho + r(1 - \rho)\nabla(k_S S_r + k_D D_r)), \quad (7)$$

$$\partial_t b = \nabla \cdot P((1 - \rho)\nabla b + b\nabla \rho + b(1 - \rho)\nabla(k_S S_b + k_D D_b)), \quad (8)$$

$$\partial_t D_r = \kappa \Delta D_r - \delta_1 D_r + r(1 - \rho), \quad (9)$$

$$\partial_t D_b = \kappa \Delta D_b - \delta_1 D_b + b(1 - \rho) \quad (10)$$

with  $x \in \Omega = [0, 1] \times [0, 1]$ ,  $t > 0$ . Appropriate boundary conditions for our application will be discussed below. Without dynamic fields, this model been analysed extensively, cf. [1, 3].

## 6. Linear Stability Analysis

We now take a closer look at the linear stability of the non-linear Nernst-Planck equations (7)-(10) with given external potentials  $S_r$  and  $S_b$ . The question is under which

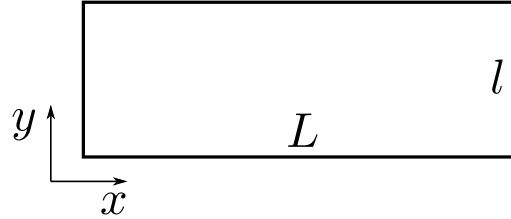


Figure 2. Geometry of the domain

conditions small perturbations in the density around the equilibrium solution do not smooth out, but are amplified in time. In our set-up, these perturbations correspond to the formation of lanes, and their frequency to the number of lanes.

To simplify the analysis, we consider cosinusoidal shaped perturbation in the  $y$  direction, hence the number of (possible) lanes is given by the mode of the cosine. We are able to predict for several densities and geometries of the domain how many lanes are formed.

From now on, we assume that the potential is acting only in  $x$ -direction. We assume the special case

$$\nabla S_r = (1, 0), \quad \nabla S_b = (-1, 0), \quad (11)$$

meaning that the red and blue persons have opposite walking directions. We assume that the diffusion of particles in  $x$ -directions vanishes, which is reasonable in case of pedestrians, as it is unlikely for them to go randomly forward or backward. On the other hand, the diffusion of  $D_i$  vanishes in  $y$ -direction, corresponding to small movements orthogonal to the walking direction. The resulting system is then given by

$$\begin{aligned}\partial_t r &= P\partial_y((1-b)\partial_y r + r\partial_y b) + Pk_S\partial_x(r(1-\rho)) \\ &\quad + Pk_D\nabla(r(1-\rho)\nabla D_r) \\ &= \nabla \cdot (-J_r)\end{aligned}\quad (12)$$

$$\begin{aligned}\partial_t b &= P\partial_y((1-r)\partial_y b + b\partial_y r) - Pk_S\partial_x(b(1-\rho)) \\ &\quad + Pk_D\nabla(b(1-\rho)\nabla D_b) \\ &= \nabla \cdot (-J_b).\end{aligned}\quad (13)$$

Hence,

$$J_r = -P \begin{pmatrix} k_S r(1-b) + k_D(r(1-\rho)\partial_x D_r \\ (1-b)\partial_y r - r\partial_y \rho + k_D(r(1-\rho)\partial_y D_r) \end{pmatrix}$$

and

$$J_b = -P \begin{pmatrix} k_S b(1-r) + k_D(b(1-\rho)\partial_x D_b \\ (1-r)\partial_y b - b\partial_y \rho + k_D(b(1-\rho)\partial_y D_b) \end{pmatrix}.$$

For the boundary conditions, we assume constant influxes of  $r$  and  $b$ . We obtain at constant influx of  $r$  and outflux of  $b$  at  $x = 0$ :

$$J_r \cdot \begin{pmatrix} -1 \\ 0 \end{pmatrix} = J_r^{in} = \text{const} \text{ and } J_b \cdot \begin{pmatrix} -1 \\ 0 \end{pmatrix} = bv_0.$$

At  $x = L$ , we obtain constant influx of  $b$  and outflux of  $r$

$$J_r \cdot \begin{pmatrix} 1 \\ 0 \end{pmatrix} = rv_0 \text{ and } J_b \cdot \begin{pmatrix} 1 \\ 0 \end{pmatrix} = J_b^{in} = \text{const}.$$

We assume no-flux boundary conditions in  $y$ -direction:

$$J_r \cdot \begin{pmatrix} 0 \\ 1 \end{pmatrix} = J_b \cdot \begin{pmatrix} 0 \\ 1 \end{pmatrix} = 0 \quad \text{for } y = 0, l.$$

We denote the equilibrium solutions by  $r^{eq}$ ,  $b^{eq}$ ,  $D_r^{eq}$  and  $D_b^{eq}$  and consider their perturbations  $r = r^{eq} + \epsilon\xi$  and  $b = b^{eq} - \epsilon\eta$ , as well as  $D_r = D_r^{eq} + \epsilon\Psi_r$  and  $D_b = D_b^{eq} - \epsilon\Psi_b$ .

This yields the following first order linearisation

$$\begin{aligned}\partial_t \xi &= P((1-b^{eq})\partial_{yy}\xi - r^{eq}\partial_{yy}\eta) \\ &\quad + Pk_S\partial_x((1-\rho^{eq})\xi - r^{eq}(\xi - \eta)) \\ &\quad + Pk_D r^{eq}(1-\rho^{eq})(\partial_{xx} + \partial_{yy})\Psi_r,\end{aligned}\quad (14)$$

$$\begin{aligned}\partial_t \eta &= P((1-r^{eq})\partial_{yy}\eta - b^{eq}\partial_{yy}\xi) \\ &\quad - Pk_S\partial_x((1-\rho^{eq})\eta - b^{eq}(-\xi + \eta)) \\ &\quad + Pk_D b^{eq}(1-\rho^{eq})(\partial_{xx} + \partial_{yy})\Psi_b,\end{aligned}\quad (15)$$

$$0 = \kappa\partial_{xx}\Psi_r - \delta\Psi_r + (1-\rho^{eq} - r^{eq})\xi + r^{eq}\eta, \quad (16)$$

$$0 = \kappa\partial_{xx}\Psi_b - \delta\Psi_b + (1-\rho^{eq} - b^{eq})\eta + b^{eq}\xi. \quad (17)$$

We denote length of the domain in  $y$ -direction by  $l$ , the length in  $x$ -direction is denoted by  $L$ , see Fig. 2. The perturbations are assumed as

$$\xi = U(x) \cos\left(\frac{k\pi}{l}y\right) \exp(\lambda t), \quad (18)$$

$$\eta = V(x) \cos\left(\frac{k\pi}{l}y\right) \exp(\lambda t), \quad (19)$$

$$\Psi_r = Y_r(x) \cos\left(\frac{k\pi}{l}y\right) \exp(\lambda t), \quad (20)$$

$$\Psi_b = Y_b(x) \cos\left(\frac{k\pi}{l}y\right) \exp(\lambda t). \quad (21)$$

where  $U(x)$ ,  $V(x)$ ,  $Y_r(x)$  and  $Y_b(x)$  denote perturbations in the  $x$ -direction, and  $k$  denotes the mode of the perturbation in  $y$ -direction. From now on, we assume  $r^{eq} = b^{eq}$ . Hence, (14) and (15) read

$$\begin{aligned}\lambda/P U &= -(1-r^{eq})\gamma U + r^{eq}\gamma V \\ &\quad + k_S(1-3r^{eq})U' + k_S r^{eq}V' \\ &\quad - k_D r^{eq}(1-2r^{eq})(\gamma + \Gamma)Y_r\end{aligned}\quad (22)$$

$$\begin{aligned}\lambda/P V &= -(1-r^{eq})\gamma V + r^{eq}\gamma U \\ &\quad - k_S(1-3r^{eq})V' - k_S r^{eq}U' \\ &\quad - k_D r^{eq}(1-2r^{eq})(\gamma + \Gamma)Y_b,\end{aligned}\quad (23)$$

where we used  $\gamma = \frac{k^2\pi^2}{l^2}$ , ' denotes the derivative with respect to  $x$ ,  $\Gamma = \frac{\pi^2}{L^2}$  and we assume perturbations  $Y_i$  of a sinusoidal or cosinusoidal type  $Y_i'' = -\Gamma Y_i$ . The equations for  $U$  and  $V$  finally read, using (16) and (17):

$$[\lambda/P + (1-r^{eq})\gamma]U - r^{eq}\gamma V \quad (24)$$

$$\begin{aligned}&+ k_D r^{eq}(1-2r^{eq})\frac{\gamma + \Gamma}{\kappa\Gamma + \delta} [(1-3r^{eq})U + r^{eq}V] \\ &= k_S(1-3r^{eq})U' + \mu r^{eq}V',\end{aligned}$$

$$[\lambda/P + (1-r^{eq})\gamma]V - r^{eq}\gamma U \quad (25)$$

$$\begin{aligned}&+ k_D r^{eq}(1-2r^{eq})\frac{\gamma + \Gamma}{\kappa\Gamma + \delta} [(1-3r^{eq})V + r^{eq}U] \\ &= -k_S(1-3r^{eq})V' - \mu r^{eq}U'.\end{aligned}$$

We denote  $\Theta = \frac{\gamma + \Gamma}{\kappa\Gamma + \delta}$ . The summation of (24) and (25) is given by

$$\begin{aligned}[\lambda/P + (1-2r^{eq})\gamma + k_D r^{eq}(1-2r^{eq})^2\Theta](U + V) \\ = k_S(1-4r^{eq})(U' - V').\end{aligned}\quad (26)$$

The derivatives of (24) and (25) are given by

$$[\lambda/P + (1-r^{eq})\gamma]U' - r^{eq}\gamma V' \quad (27)$$

$$\begin{aligned}&+ k_D r^{eq}(1-2r^{eq})\Theta [(1-3r^{eq})U' + r^{eq}V'] \\ &= k_S(1-3r^{eq})U'' + \mu r^{eq}V'',\end{aligned}$$

$$[\lambda/P + (1-r^{eq})\gamma]V' - r^{eq}\gamma U' \quad (28)$$

$$\begin{aligned}&+ k_D r^{eq}(1-2r^{eq})\Theta [(1-3r^{eq})V' + r^{eq}U'] \\ &= -k_S(1-3r^{eq})V'' - \mu r^{eq}U''.\end{aligned}$$

and their difference gives

$$\begin{aligned} & [\lambda/P + \gamma + k_D r^{eq}(1 - 2r^{eq})(1 - 4r^{eq})\Theta](U' - V') \\ & = k_S(1 - 2r^{eq})(U'' + V''). \end{aligned} \quad (29)$$

Combining (26) and (29) leads to

$$[\lambda/P + (1 - 2r^{eq})\gamma + k_D r^{eq}(1 - 2r^{eq})^2\Theta](U + V) = \quad (30)$$

$$k_S^2 \frac{(1 - 4r^{eq})(1 - 2r^{eq})}{\lambda/P + \gamma + k_D r^{eq}(1 - 2r^{eq})(1 - 4r^{eq})\Theta}(U'' + V'').$$

In the following, we assume perturbations  $U$  and  $V$  in  $x$ -direction of a sinusoidal type, due to the homogeneous boundary conditions. This leads to

$$U'' = -\frac{m^2\pi^2}{L^2}U, \quad V'' = -\frac{m^2\pi^2}{L^2}V,$$

where  $L$  denotes the length of the domain in  $x$  direction. In the following, we take  $m = 1$ , as we are only interested in lanes forming along the  $x$ -direction. We finally arrive at

$$\begin{aligned} & [\lambda^2/P^2 + 2\lambda/P[\gamma(1 - r^{eq}) + k_D r^{eq}(1 - 2r^{eq})(1 - 3r^{eq})\Theta] \\ & + \gamma^2(1 - 2r^{eq}) + 2\gamma k_D r^{eq}(1 - 2r^{eq})^3\Theta \\ & + k_D^2 r^{eq2}(1 - 2r^{eq})^3(1 - 4r^{eq})\Theta^2 \\ & + k_S^2\Gamma(1 - 4r^{eq})(1 - 2r^{eq})](U + V) = 0. \end{aligned} \quad (31)$$

Accordingly, the equation for  $\lambda$  is given by

$$\begin{aligned} \lambda_{1/2} = & -P[(1 - r^{eq})\gamma + k_D r^{eq}(1 - 2r^{eq})(1 - 3r^{eq})\Theta] \\ & \pm P\sqrt{r^{eq2}[\gamma - k_D r^{eq}(1 - 2r^{eq})\Theta]^2} \\ & - k_S^2\Gamma(1 - 4r^{eq})(1 - 2r^{eq})}. \end{aligned} \quad (32)$$

$\lambda$  is supposed to be real-valued for all  $k$ , particularly for  $k = 1$ . From that we conclude

$$r^{eq2}[\gamma - k_D r^{eq}(1 - 2r^{eq})\Theta]^2 \geq k_S^2\Gamma(1 - 4r^{eq})(1 - 2r^{eq}) \quad (33)$$

As  $r^{eq} \leq 1/2$ , (33) is always fulfilled in case that  $r^{eq} \geq 1/4$ . This means that instabilities arise only in case  $r^{eq} \geq 1/4$ .

To obtain instabilities increasing in time,  $\lambda > 0$  has to be satisfied. This means

$$\begin{aligned} & [(1 - r^{eq})\gamma + k_D r^{eq}(1 - 2r^{eq})(1 - 3r^{eq})\Theta]^2 \\ & < r^{eq2}\gamma^2 - 2\gamma k_D r^{eq}r^{eq3}(1 - 2r^{eq})\Theta \\ & + k_D^2 r^{eq4}(1 - 2r^{eq})^2\Theta^2 - k_S^2\Gamma(1 - 4r^{eq})(1 - 2r^{eq}) \end{aligned} \quad (34)$$

Assuming  $(1 - 2r^{eq}) > 0$ , which means that the overall density is below maximum, we obtain

$$\begin{aligned} & \gamma^2 + 2\gamma k_D r^{eq}(1 - 2r^{eq})^2\Theta \\ & + k_D^2 r^{eq2}(1 - 2r^{eq})^2(1 - 4r^{eq})\Theta^2 + k_S^2\Gamma(1 - 4r^{eq}) < 0. \end{aligned} \quad (35)$$

The mode of the cosinusoidal perturbation in  $y$ -direction is given by  $k$ , hence it gives the number of lanes of particles moving in opposite direction which are amplified during time. If  $k = 1$ , we obtain one lane in each direction.

Accordingly, we obtain as inequality for  $\gamma = \frac{k^2\pi^2}{l^2}$

$$\begin{aligned} & \gamma^2 \left[ 1 + 2k_D r^{eq}(1 - 2r^{eq})^2 \frac{1}{\kappa\Gamma + \delta} \right. \\ & \left. + k_D^2 r^{eq2}(1 - 2r^{eq})^2(1 - 4r^{eq}) \frac{1}{(\kappa\Gamma + \delta)^2} \right] \\ & + \gamma \left[ 2k_D r^{eq}(1 - 2r^{eq})^2 \frac{\Gamma}{\kappa\Gamma + \delta} \right. \\ & \left. + 2k_D^2 r^{eq2}(1 - 2r^{eq})^2(1 - 4r^{eq}) \frac{\Gamma}{(\kappa\Gamma + \delta)^2} \right] \\ & + k_D^2 r^{eq2}(1 - 2r^{eq})^2(1 - 4r^{eq}) \frac{\Gamma^2}{(\kappa\Gamma + \delta)^2} + k_S^2\Gamma(1 - 4r^{eq}) \end{aligned} \quad (36)$$

$< 0$ .

The evaluation of (36) leads to a condition on  $k$  which determines under which conditions instabilities, which lead to lane formation, appear.

## 6.1. Number of Lanes for varying Density

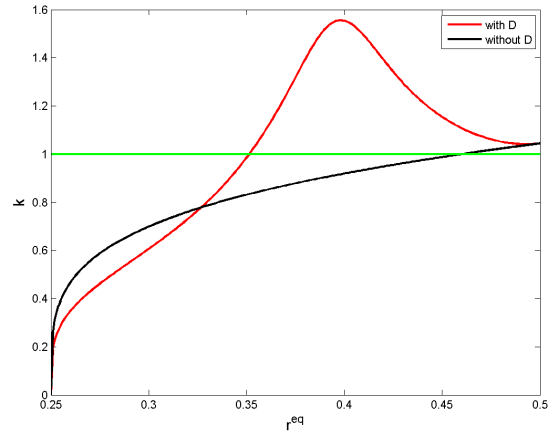


Figure 3. Number of lanes versus density

We are able to predict instabilities, thus forming of lanes and the number of lanes, depending on the density  $r^{eq}$ . In Figure 3, the number of lanes  $k$  is plotted versus the density  $r^{eq}$ . In this setup, we choose as length  $l$  in  $y$ -direction 7 m. The length  $L$  in Figure 3 is 100 m. The decrease  $\delta$  is given by 0.05, and  $k_D = 1$ . We set  $k_S = 7$ . Without the dynamic fields  $D_i$ , the first lane in each direction arises at densities of approximately 0.45 in each direction. If we consider the dynamic fields, the first lanes are formed at densities of approximately 0.35. Hence, the inclusion of the dynamic fields leads indeed to an increase of the tendencies to follow others.

## 6.2. Number of Lanes for varying Length

Figure 4 shows the number of lanes plotted versus length  $L$ . We chose the same parameters as before, the density is set to  $r^{eq} = 0.33$ . It is obvious that the herding behaviour

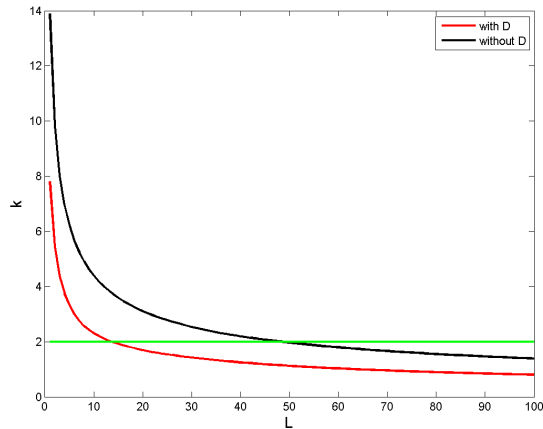


Figure 4. Number of lanes versus length  $L$

does not lead to an increase in lanes. As expected, the tendency to follow others is more pronounced, this results in less lanes.

## 7. Conclusion & Future Work

We demonstrated the lane formation capabilities of an extended floor field model. Using the link of this model to a macroscopic PDE, we were able to give conditions on the formation of lanes depending on the density of particles as well as the geometry on the domain. The effect of the floor field presenting herding behaviour is that lanes are formed at lower densities. A logical next step would be to systematically verify these condition using the Monte Carlo simulations described above. Also, it would be worthwhile to perform detailed simulation on the macroscopic model (using, e.g. a finite difference scheme) and to compare these results with the microscopic simulations. This would lead to a unified understanding of lane formation in these kinds of models.

## References

- [1] M. Burger, M. Di Francesco, J.-F. Pietschmann, and B. Schlake. Nonlinear cross-diffusion with size exclusion. *SIAM Journal on Mathematical Analysis*, 42(6):2842–2871, 2010.
- [2] M. Burger, P. Markowich, and J.-F. Pietschmann. Continuous limit of a crowd motion and herding model: Analysis and numerical simulations. submitted, 2011.
- [3] M. Burger, B. Schlake, and W. M.-T. Nonlinear Poisson-Nernst Planck Equations for Ion Flux through Confined Geometries. *preprint*, 2010.
- [4] C. Burstedde, K. Klauck, A. Schadschneider, and J. Zittartz. Simulation of pedestrian dynamics using a two-dimensional cellular automaton. *Physica A: Statistical Mechanics and its Applications*, 295(3-4):507–525, 2001.
- [5] M. Fukui and Y. Ishibashi. Self-organized phase transitions in CA-models for pedestrians. *J. Phys. Soc. Japan*, 8:2861–2863, 1999.
- [6] D. Helbing. Traffic and related self-driven many-particle systems. *Rev. Mod. Phys.*, 73(4):1067–1141, Dec 2001.
- [7] D. Helbing, I. Farkás, P. Molnár, and T. Vicsek. *Simulation of pedestrian crowds in normal and evacuation situations*, pages 21–58. Schreckenberg, M. and Sharma, S.D., 2002.
- [8] D. Helbing, I. Farkas, and T. Vicsek. Freezing by heating in a driven mesoscopic system. *Physical Review Letters*, 84:1240–1243, 2000.
- [9] D. Helbing, I. J. Farkas, P. Molnar, and T. Vicsek. Simulation of pedestrian crowds in normal and evacuation situations. in: *M. Schreckenberg and S. D. Sharma (eds.) Pedestrian and Evacuation Dynamics (Springer, Berlin)*, pages 21–58, 2002.
- [10] D. Helbing and P. Molnár. Social force model for pedestrian dynamics. *Phys. Rev. E*, 51(5):4282–4286, 1995.
- [11] A. Kirchner. Modellierung und statistische Physik biologischer und sozialer Systeme. PhD Thesis (in german), 2002.
- [12] A. Kirchner and A. Schadschneider. Simulation of evacuation processes using a bionics-inspired cellular automaton model for pedestrian dynamics. *Physica A: Statistical Mechanics and its Applications*, 312(1-2):260 – 276, 2002.
- [13] M. Matsumoto and T. Nishimura. Mersenne twister: a 623-dimensionally equidistributed uniform pseudo-random number generator. *ACM Trans. Model. Comput. Simul.*, 8(1):3–30, 1998.
- [14] M. Muramatsu and T. Nagatani. Jamming transition in two-dimensional pedestrian traffic. *Physica A*, 275:281 – 291, 2000.
- [15] A. Schadschneider. Simulation of evacuation processes using a bionics-inspired cellular automaton model for pedestrian dynamics. In M. Fukui, Y. Sugiyama, M. Schreckenberg, and D. Wolf, editors, *Traffic and Granular Flow 01*, pages 499–511. Springer-Verlag Berlin Heidelberg, Nagoya, 2002.
- [16] A. Schadschneider, W. Klingsch, H. Kluepfel, T. Kretz, C. Rogsch, and A. Seyfried. *Encyclopedia of Complexity and System Science*, R. A. Meyers, (ed.), volume 3, chapter Evacuation Dynamics: Empirical Results, Modeling and Applications, page pp. 3142. Springer, 2009.
- [17] M. Simpson, K. Landman, and B. Hughes. Diffusing populations: ghosts or folks? *Australasian Journal of Engineering Education*, 15:59–67, 2009.
- [18] A. Sopasakis and M. A. Katsoulakis. Stochastic modeling and simulation of traffic flow: Asymmetric single exclusion process with arrhenius look-ahead dynamics. *SIAM Journal on Applied Mathematics*, 66(3):921–944, 2006.
- [19] A. Treuille, S. Cooper, and Z. Popovic. Continuum crowds. In *ACM Transaction on Graphics*, volume 25, pages 1160–1168, 2006. Proceedings of SCM SIGGRAPH 2006.
- [20] U. Weidmann. Transporttechnik der Fussgänger - Transporttechnische Eigenschaften des Fussgängerverkehrs (Lit-

eraturstudie). Literature Research 90, Institut für Verkehrsplanung, Transporttechnik, Strassen- und Eisenbahnbau IVT an der ETH Zürich, March 1993. in German.

- [21] S. J. Yuhaski, Jr. and J. M. Smith. Modeling circulation systems in buildings using state dependent queueing models. *Queueing Systems Theory Appl.*, 4(4):319–338, 1989.